Grey-box Modeling of Reversible Solid Oxide Cell Stack's Electrical Dynamics Based on Electrochemical Impedance Spectroscopy

Jessen, Kasper; N. Soltani, Mohsen; Hajizadeh, Amin; Jensen, Søren Højgaard; Schaltz, Erik; Nielsen, Martin N.; Smitshuysen, Thomas Lyck

Published in:
2023 IEEE Conference on Control Technology and Applications (CCTA)

Publication date:
2023

Document Version
Accepted author manuscript, peer reviewed version

2023 IEEE Conference on Control Technology and Applications (CCTA)
August 16-18, 2023. Bridgetown, Barbados

Grey-box Modeling of Reversible Solid Oxide Cell Stack's Electrical Dynamics Based on Electrochemical Impedance Spectroscopy

Kasper Jessen[1], Mohsen Soltani[1] , Amin Hajizadeh[1], Søren H. Jensen[2,3], Erik Schaltz [3], Martin N. Nielsen[2] and Thomas E. L. Smitshuysen[2]

***Abstract*—This paper aims to design a lumped-capacity model of a reversible solid oxide cell stack for hydrogen electrolysis. The lumped-capacity model needs to have an adequate representation of the electrical dynamics over a wide operating range and a model structure suitable for the design of a physical emulator. The grey-box model is based on data obtained by electrochemical impedance spectroscopy conducted on a commercial solid oxide cell stack for four different gas compositions at six aging stages. In addition, a comparison of the experimental and simulated voltage response of the reversible solid oxide cell stack in cyclic reversible operation mode was conducted at different aging levels of the stack.**

***Index Terms*—System Identification, Grey-box modeling, Electrochemical Impedance Spectroscopy, Electrolysis**

I. Introduction

The growing energy consumption and climate concerns have given rise to an increasing number of renewable energy resources. To utilize as much of the electricity from fluctuating renewable energy resources as possible, a promising solution is electrolysis to produce hydrogen [1]. The hydrogen produced during the electrolysis process can be used as a medium for energy storage and for applications such as producing heat for buildings, refueling fuel cell vehicles, and as a source of feedstock for industry [2].

Three main types of water electrolysis technology exist and can be distinguished by their charge carrier and electrolyte: alkaline, proton exchange membrane, and solid oxide. The alkaline and proton exchange membrane electrolysers are mature technologies that are currently employed in large-scale plants, whereas Solid Oxide Cell (SOC) technology is less mature.

The SOC technology can be used both for fuel cells and electrolysers. The same SOC can often be used for both operations modes, denoted as a Reversible Solid Oxide Cell (RSOC). The SOC has the highest energy efficiency potential for hydrogen production and also offers syngas production via co-electrolysis. However, the SOC electrolyser technology suffers high cost and insufficient long-term durability, particularly at high current densities, which currently hinders this technology scaling possibility [3], [4].

It has been proposed in [5], that the electrolysis-induced degradation of a RSOC caused by steam electrolysis continuously at high current density could be reduced by reversible cycling between electrolysis and fuel cell modes. It was shown that the degradation at cell level when applying reversibly cycling was essentially eliminated for an 1100 h test. Furthermore, it was revealed that the degradation reduction depended on the hourly periods of operation modes between cycling.

Recently, a new operation mode for RSOC electrolysers was proposed in [6], where the conventional galvanostatic or potentiostatic SOC electrolysis operation is substituted with a pulsed operation where an AC current (or voltage) is applied on top of a DC current (or voltage), an operating mode referred to as AC:DC operation. The AC:DC operation involves cycling asymmetrically around the Open-Circuit Voltage (OCV) of the RSOC, with cycling periods in the order of a couple of milliseconds. By operating most of the time in the electrolysis mode, this can be used for hydrogen production. The AC:DC method has been experimentally validated and showed that the temperature profile across the cell could be kept flat which reduces thermal stress on the cell. Furthermore, experimental tests showed that the AC:DC method potentially minimizes the degradation caused by impurities and nickel migration. This could result in a simple way to achieve increased RSOC stack module sizes and extended lifetime.

However, before implementing the novel AC:DC operational mode for RSOC for electrolysis on a large scale, an investigation of the associated Power Electronic Converters (PEC) is required for the cyclic bidirectional operation mode and the grid integration. Furthermore, a fast and robust control system is required to ensure the tracking performance of the defined AC:DC current references for the PEC. All this is to ensure the performance of the system in terms of stability, efficiency, and reliability.

The main contribution of this paper is to determine a method to find a suitable model which can reproduce the electrical dynamic behavior of a reversibly cycled (AC:DC operated) RSOC stack from experimental data obtained by

*This work is a part of the DynAmmonia and DynEfuel projects both supported by EUDP with grant numbers 64021-3104 and 640222-496142.

[1] are with the department of Energy, Aalborg University, 6700 Esbjerg, Denmark kje@et.aau.dk

[2] are with the company Dynelectro ApS, 4130 Viby Sjælland, Denmark

[3] are with the department of Energy, Aalborg University, 9000 Aalborg, Denmark

Electrochemical Impedance Spectroscopy (EIS). The lumped capacity model can be used as a basis for a wide range of applications, such as; Control design for PEC and real-time implementations such as performance predictions, fault detection, state of health monitoring and diagnostics. Furthermore, a suitable model can be used to design a physical emulator for the stack, which can reproduce the electrical behavior of the real system. An RSOC stack emulator allows for experimental investigation of a single or multiple RSOC stacks and the associated PEC and control systems. Thereby, an experimental pre-validation can be made before implementation in the real system which could cause expensive damages to the RSOC stacks.

This paper is organized as follows, section II gives a short review of the different analysis and modeling methods for SOC. Section III describes the choice of model structure and the parametrization from experimental EIS data. Section IV a time-domain simulation of the developed RSOC stack model is conducted in MATLAB/Simulink and is compared against experimental data from the RSOC in AC:DC electrolysis operation mode. In the last section V, is the conclusion of the paper.

II. Modeling of the RSOC stack

The SOC are complicated systems containing multiple mass-transfer, chemical, and electrochemical processes, the coupling of these makes the system non-linear. Therefore, different modeling techniques for SOC systems have been utilized for different aspects. Extensive reviews of the SOC modeling techniques can be found in [7], [8]. In [9], the challenges associated with developing a unified model, and how to overcome them are discussed.

The white-box or physical modeling approach is used for cell design modification or material development, but it is used as a primary tool to understand cell performance for system analysis. The physical modeling approach utilizes the knowledge of physic-chemical characteristics and employs computational fluid dynamics to simulate all the relevant heat, mass, and charge transfer processes.

The black-box model is a model that is based on an extensive amount of experimental data from the system and have no prior model informationion available. An RSOC model can be derived through a statistical data-driven approach. The black-box model is constructed without any physical laws, which simplifies the complexity of the model. This modeling approach is mainly used for the design of model-based control systems.

The Equivalent Circuit Model (ECM) for electrochemical systems is a gray-box system identification approach, which is also an experimental data-driven method that usually uses data obtained by EIS and a predetermined model structure in the form of an ECM.

EIS is a method of measuring the impedance of an electrochemical system at different frequencies. This is often conducted using a Frequency Response Analyzer (FRA), which excites the system with a small sinusoidal voltage or current perturbation and measures the response at a single operating point [10]. The EIS data can be visualized through Nyquist or Bode plots to gain insight into the system behavior at the operating point for different frequencies. The EIS data can be used to parametrize an ECM, utilizing an algorithm to identify the structure and/or parameters of the ECM. The parameters of the ECM are often used to provide a physical interpretation of SOC mass transport, reaction rates, electrolyte resistance, etc. [11]. In [12], it was shown that the idea of fitting serially connected parallel coupled pairs of resistor and capacitor (RC elements) to a measured impedance spectrum could be done for every possible non-oscillating electrochemical process.

In this paper, the ECM approach is chosen as the modeling approach, with a parametrization of lumped ideal RC elements. This approach provides a good candidate to develop a lumped capacity model, which is also a suitable model for a physical emulator. The parameterization of the ECM is conducted based on experimental data obtained from EIS at OCV on a commercial RSOC stack from SolydEra SpA with a nominal electrolysis and fuel-cell capacity of 4.5kW and 1.5 kW, respectively. The RSOC stack was continuously operated in AC:DC electrolysis mode at a temperature of around 750°C. However, at regular intervals, an EIS test was performed at different gas flow compositions at 700°C at OCV. The EIS data obtained provide a good description of the system dynamics at different operating conditions and levels of aging over a wide frequency range.

III. System Identification of RSOC

The system identification of the RSOC stack is based on the impedance spectrum data from the EIS conducted at four different gas flow ratio experiments, at six different time instances, where aging of the RSOC stack has occurred.

The impedance spectra measured for the RSOC stack can be seen in Fig. 2, and the gas flow mixtures used in the experiments can be seen in Table I. The EIS was conducted using an FRA from 0.1 Hz to 100 kHz with 71 frequency sample points at OCV.

EIS can only be used to analyze a system, which satisfies the conditions of causality, linearity, and stability. To check the fulfillment of these conditions for the system, the Kramers-Kronig (K-K) relations are used. The K-K relations consist of a set of transformations that can be used to predict one part of the impedance from the other [13]. A residual spectrum can be calculated by comparing the predicted and measured parts of the impedance spectrum, which should be small to fulfill the requirements. The K-K relations test in [14], was used on all the measured impedance spectra data and all residual spectra had small residual values within the limits. The residual spectra are not shown in this paper.

From the inspection of impedance spectra characteristics in Fig. 2, it can be seen that from the low-frequency range, two impedance drops occur. At the end of the measurement range, an approximately constant impedance occurs. The analogy in electrical circuit elements for these impedance spectra can be described by an ECM where two RC elements and a single resistor are connected in series. The electrical circuit model

TABLE I
GAS FLOW MIXTURE FOR THE EIS EXPERIMENTS CONDUCTED AT A TEMPERATURE OF 700°C.

	Exp. 1	Exp. 2	Exp. 3	Exp. 4
H_2O [g/min]	27	23	23	23
H_2 [NL/min]	3	6	6	6
Air [NL/min]	372	100	200	372
N_2 [NL/min]	0	75	0	0

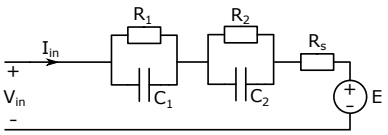

Fig. 1. The electrical circuit of the model.

can be seen in Fig. 1, and it consists of the ECM and a voltage source E. The voltage source represents the OCV the RSOC stack generates.

The nominal OCV of the RSOC stack was determined as the mean of the OCV voltage measurements, which were conducted before each EIS experiment. The measured OCV at both temperatures showed a spread with a small range ($< \pm$ 2V) around the nominal OCV. The impedance spectra show a large phase lead at the high-frequency range, and this is due to the inductance of the current collector wires, but mainly due to the inductance of the cables connecting the RSOC stack to the FRA equipment, which differs between the six ages. However, the inductance is neglected in the model due to the limited amount of additional information it would add to the dynamic model of the RSOC stack, due to a low value of inductance, and most of the inductance is thought to originate from the wiring of the RSOC stack to the FRA equipment. The dynamics of the chosen ECM structure can be described by the differential equations in eq. 1

$$\begin{aligned} C_1\frac{dv_{c1}(t)}{dt} &= I_{in} - \frac{v_{c1}(t)}{R_1} \\ C_2\frac{dv_{c2}(t)}{dt} &= I_{in} - \frac{v_{c2}(t)}{R_2} \\ V_{in}(t) &= v_{c1}(t) + v_{c2}(t) + I_{in}(t)R_s \end{aligned} \tag{1}$$

where C_1 and C_2 are the capacitors and v_{c1} and v_{c2} are the voltage across C_1 and C_2, respectively. R_1, R_2, and R_s are the resistors. V_{in} and I_{in} are the input voltage and current of the ECM, respectively. To identify the parameters, the equations in eq. 1 are converted to a state-space model in eq. 2.

$$\begin{aligned} \mathbf{A} &= \begin{bmatrix} \frac{-1}{C_1R_1} & 0 \\ 0 & \frac{-1}{C_2R_2} \end{bmatrix}, & \mathbf{x}(t) &= \begin{bmatrix} v_{c1}(t) \\ v_{c2}(t) \end{bmatrix} \\ \mathbf{B} &= \begin{bmatrix} \frac{1}{C_1} \\ \frac{1}{C_2} \end{bmatrix}, & u(t) &= \begin{bmatrix} I_{in}(t) \end{bmatrix} \\ \mathbf{C} &= \begin{bmatrix} 1 & 1 \end{bmatrix}, & y(t) &= \begin{bmatrix} V_{in}(t) \end{bmatrix} \\ D &= \begin{bmatrix} R_s \end{bmatrix} \end{aligned} \tag{2}$$

In this paper, the unknown parameters of the model are the five electrical parameters: C_1, C_2, R_1, R_2, and R_s. To identify these, a grey-box modeling approach is utilized, as some of the entries in the state-space model in eq. 2 are known due to the model structure.

The identification of the five electrical parameters is accomplished by minimizing the error between the model impedance and the measured impedance data. A cost function is defined in eq. 3 for the model in the frequency domain [15].

$$V(\boldsymbol{\theta}) = \sum_{j=1}^{\mathrm{N}} \|Z(\omega_j) - G(\boldsymbol{\theta}, \omega_j)\|^2 \, \|U(\omega_j)\|^2 \tag{3}$$

Where V is the cost function for the model. $\boldsymbol{\theta}$ is the parameter vector, ω_j is the frequency at the sample j, and N is the number of samples. Z is the measured impedance data, and U is the input excitation data. G is the transfer function of the time-domain model in eq. 2. Thus, to estimate the parameter vector, a minimization between the measured impedance $Z(\omega_j)$ and the transfer function value $G(\boldsymbol{\theta}, \omega_j)$. The parameter vector estimation is thereby formulated as a minimization problem in eq. 4.

$$\hat{\boldsymbol{\theta}} = \arg\min_{\boldsymbol{\theta}} V(\boldsymbol{\theta}) \tag{4}$$

For the numerical minimization of the function $V(\boldsymbol{\theta})$, the Gauss-Newton iterative search method is applied [15]. The iterative numerical minimization method requires an initial set of model parameters. Due to the physical insight of the system from the impedance spectra, an initial model parameter set was estimated, the initial parameters used was C_1= 0.8 F, $C_2 = 0.40$ mF, and R_1=R_2=R_s= 0.2 Ω.

The impedance spectra of the twenty different fitted models are shown in a Bode plot visualization with dashed lines in Fig. 2 with the corresponding experimental impedance spectra as solid lines. By examination of the difference between the measured impedance spectra and the corresponding fitted models impedance spectra, a similarity is seen in the impedance magnitude across the measured frequency range, but for the phase angle a discrepancy is seen at frequencies above 400 Hz due to the missing inductance term in the fitted models. However, the fitted models still have a fit percentage to the measured EIS data with a mean fit percentage of 85.9% with a standard deviation of 1.4%.

From each of the fitted models, there are five estimated electrical parameters. A data set for each electrical parameter can be obtained from the different fitted models. For graphically displaying the statistics of each electrical parameter data set, a box plot is employed in Fig. 3. The box plot shows the median and mean of each electrical parameter data set. The bottom and top of each blue box are the 25th and 75th percentiles. This range is also denoted as the Inter Quartile Range (IQR), and the whiskers extension displays the most extreme data points not considered outliers.

From the box plots, it can be seen that the data set for each electrical parameter have a different relative range of estimates compared to the median. The IQR is relatively small around the median of the estimated capacitors , whereas it is almost double the relative size for the estimates of the resistors. There are two outliers observed in the box plot of

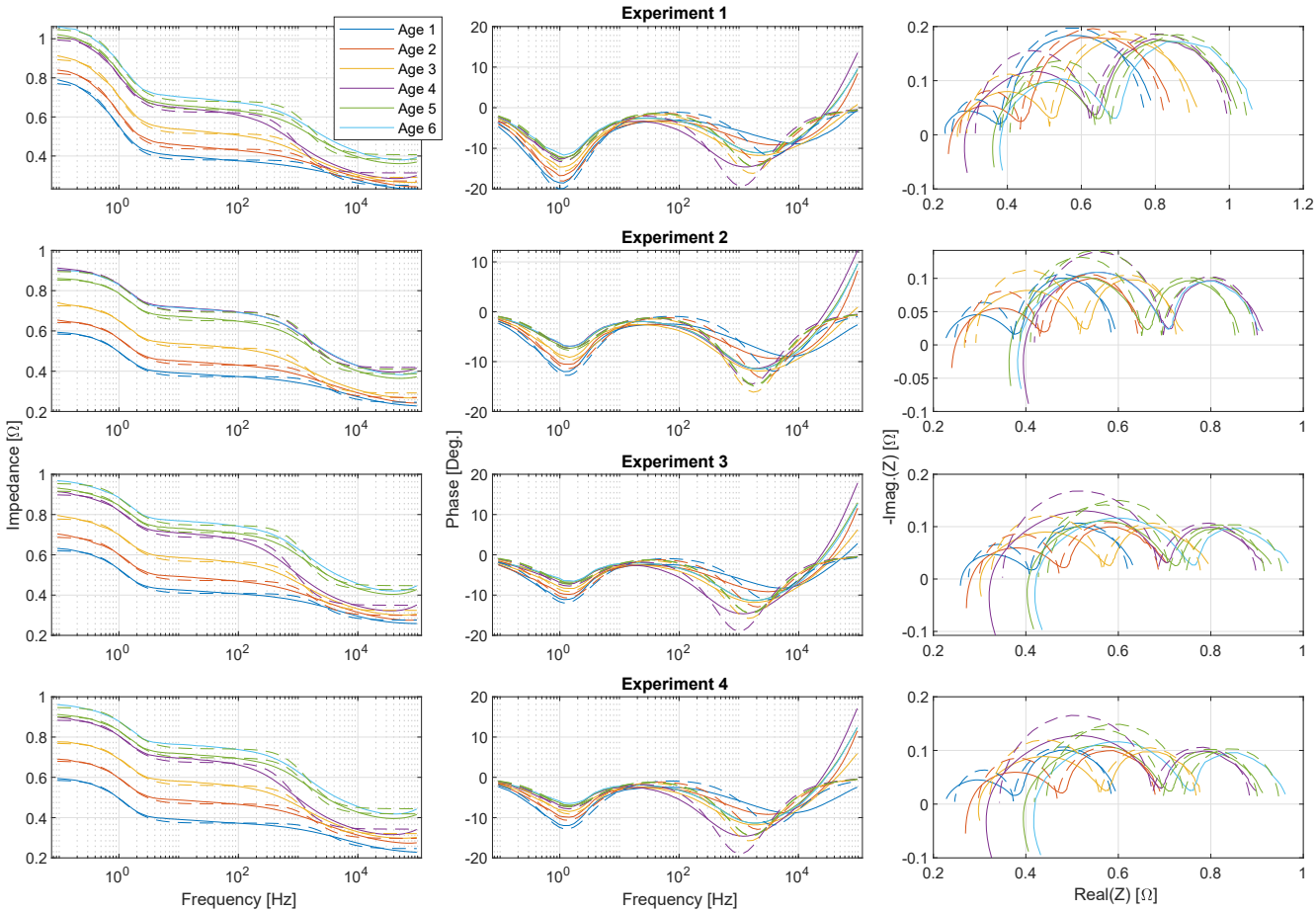

Fig. 2. The experimental EIS data is shown as solid lines, whereas the corresponding fitted models data are shown as dashed lines.

the data set for the C_1 capacitance. The outliers are due to the operating conditions in experiment 1. This can also be seen in Fig. 2 for experiment 1, where the magnitude and phase at low frequencies, have a relatively larger deviation from the other experiments compared to each other.

A statistical evaluation of the box plot is necessary to determine the five electrical parameters for the nominal ECM for the RSOC stack. For the electrical parameters C_1, C_2, R_2, and R_s only a slight relative skewness in the distribution of the electrical parameter set is noticed by comparing the center of the IQR and the median. For the electrical parameter R_1, a large skewness in the distribution of the electrical parameter set is observed. The skewness of R_1 is due to the large impedance at low-frequency region in experiment 1 compared to the other experiments. Due to the small sample size for each parameter and the observed outliers, the median is chosen as a robust statistical evaluation of the central tendency of the estimated parameter sets for the parametrization of the nominal model. The confidence interval for the chosen parameter is not used in this paper, due to the skewness, non-normal distribution and low sample number for the estimated electrical parameter sets. However, the boxplot give a good insight into the uncertainty of the electrical parameters in the model, which is valuable for future system robustness analysis. The five electrical parameters for the nominal dynamical model of the RSOC stack can be seen in Table II.

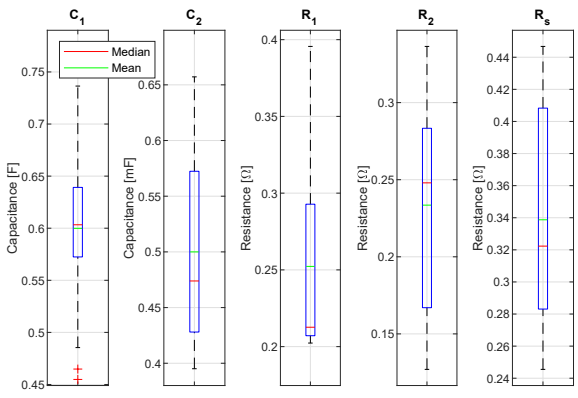

Fig. 3. Box plot of estimated electrical parameter data sets for 700°C.

A. Operating Temperature Effect

Changing the RSOC stack operating temperature impacts the dynamics of the system. The EIS was conducted at 700°C, except at age 6 where it was also conducted at 750°C, whereas the continuous AC:DC operation of the RSOC stack is conducted near 750°C. In [16], [17], the variation in performance due to temperature was investigated for the same type of RSOC used in this paper and it was shown in that the

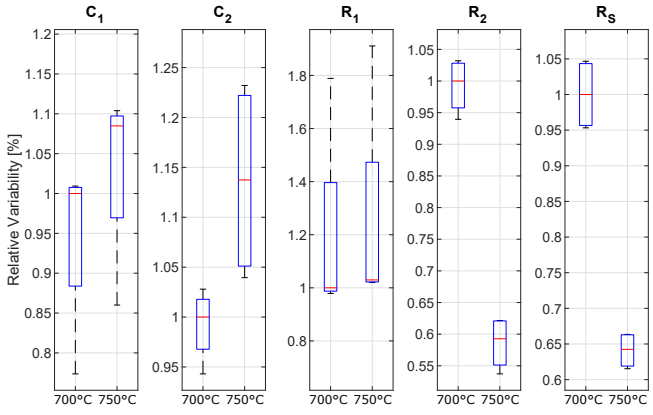

Fig. 4. Box plot visualizing the ratio of the estimated electrical parameter data sets relative to the median of the parameter estimate at 700°C at age 6 for the two operating temperatures.

TABLE II
ELECTRICAL PARAMETERS FOR THE NOMINAL ECM OF THE RSOC STACK AT THE TWO OPERATING TEMPERATURES.

Temp.[°C]	C_1[F]	C_2[mF]	$R_1[\Omega]$	$R_2[\Omega]$	$R_s[\Omega]$	E[V]
700	0.61	0.47	0.21	0.25	0.32	63
750	0.61	0.47	0.21	0.15	0.20	61

dominant effect of increasing the temperature was a reduction in the ohmic resistance. The ohmic reduction was due to an improved ionic conductivity of the electrolyte, barrier layer, and cathode. In [16, Fig. 1], an exponential fit from experimental data gives a function for the area-specific ohmic resistance dependence on the inverse of the temperature. The function estimates that changing the operating temperature from 700°C to 750°C results in an approximately 35 % reduction in the area-specific ohmic resistance.

To relate the estimated electrical nominal parameters estimated at 700°C to the electrical parameters for the nominal dynamical model at 750°C an investigation of the relative ratio between the estimated electrical parameter data sets to the median of each parameter data sets median at 700 °C at age 6 are conducted in Fig. 4. The effect of the operating temperature is mainly affecting the ohmic resistance for the electrical parameters R_2 and R_s with a decrease 41% and 36%, respectively. The correlation found between the ohmic resistance and temperature is used to calculate the electrical parameters for the nominal dynamical model at 750°C.

IV. Model Validation

The experimental data consists of a set of time domain measurements of the stack voltage and current at the different ages studied. The measurements were sampled at 100 kHz. Unfortunately, the time domain data from age 1 was corrupted, so no comparisons were conducted for this age.

To validate the dynamic performance of the nominal electrical circuit model, it was constructed in MATLAB Simulink using the Simscape Specialized Power Systems toolbox. As the experimental current excitation is not a perfect square waveform, the simulation model utilizes the experimental current measurement as input. The comparison of the time domain measurements in AC:DC operation between the experimental and simulation can be seen in Fig. 5.

The contentious operation of the stack is conducted at nominal operating conditions, which is a temperature of around 750°C with a gas flow ratio of 1500 g/h H_2O and 14.7 NLM H_2. The continuous AC:DC operation was in some of the experiments conducted with different frequencies and duty ratios. At ages 2 and 3 the AC:DC operation is shown at a frequency of 100 Hz with a duty ratio of 80% electrolysis mode. At ages 4 and 5 the AC:DC operation shown was conducted with a frequency of 60 Hz with a duty ratio of 88 % electrolysis mode. At age 6 the AC:DC operation shown was conducted with a frequency of 30 Hz with a duty ratio of 90 % electrolysis mode. A bidirectional power supply generated the asymmetric square-shaped excitation waves.

The time domain dynamic comparison shows an agreement in the transient response at the different aging levels of the RSOC stack. However, a DC-gain difference can be seen in the early ages. This is as expected, as there is a variation in the resistances at the different aging stages, and the simulation model only uses the nominal values determined for the resistances in the model. Furthermore, a part of the DC-gain difference is expected to occur due to a higher fuel utilization the AC:DC operation than during the EIS, which increases the value of the estimated resistances [18].

V. Conclusion

Initially, an experimental analysis of the dynamics of the RSOC was conducted using EIS at four different gas flow ratios, conducted at six different aging levels of the RSOC stack. From the experimentally obtained impedance spectra, a suitable ECM structure was chosen to consist of two parallel RC elements and a single resistor connected in series. The parameters were estimated using a gray-box system identification method by utilizing the developed mathematical model of the chosen ECM and the obtained EIS data.The distribution of the parameterization data sets was visualized by a box plot, from which the nominal parameters of the equivalent circuit were chosen. The electrical circuit model using the nominal estimated parameters was used for simulation of the time dynamics, which showed an overall good agreement in the transient response compared to experimental data from the RSOC stack in AC:DC operation at the different aging stages. However, a larger DC-gain difference was found for the early degradations stages.

This paper presents a method to derive a lumped capacity model which describes the electrical behavior for an RSOC stack that can be derived using the widely used EIS data and ECM approach. This method is generalizable for other RSOC stacks, and the same model structure can be used for other RSOC having a similar impedance characteristics.

The model presented in this paper, will be used for future work in developing a physical emulator of the RSOC stack. Furthermore, it will be used for the control design and performance validation for a PEC supplying a RSOC stack in AC:DC operation mode.

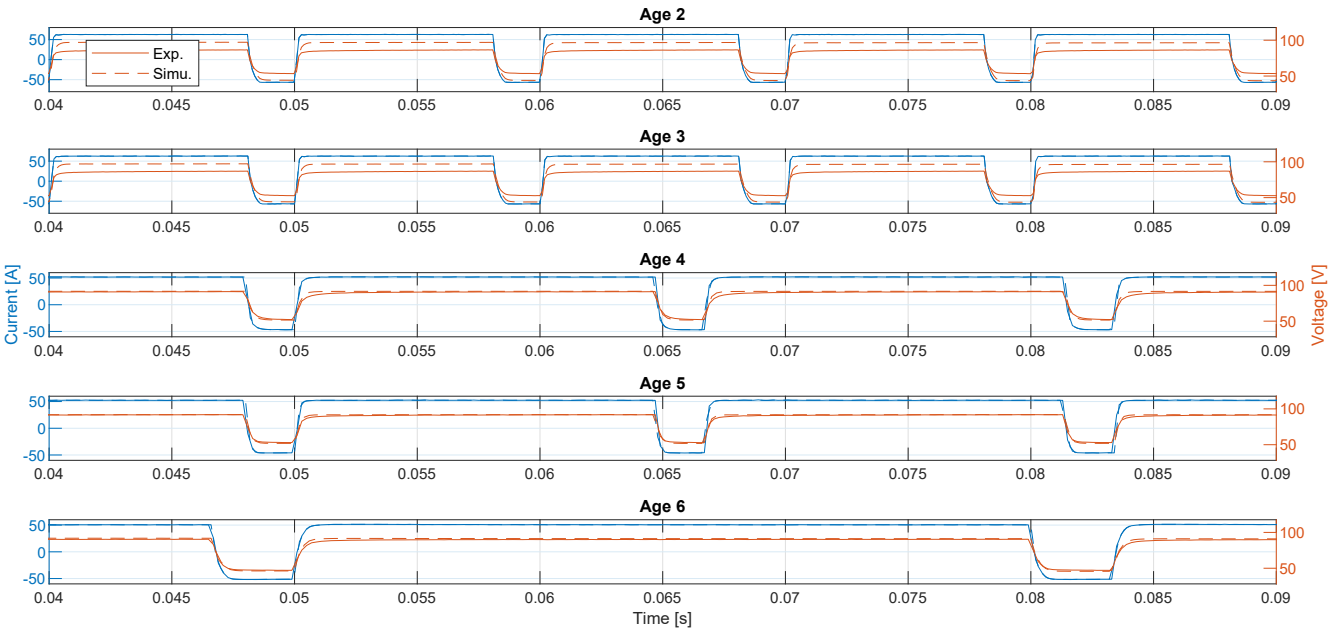

Fig. 5. Comparison of current and voltage measurements from the RSOC stack and simulation in AC:DC operation mode.

REFERENCES

[1] IEA, "World Energy Outlook 2022," Paris, Tech. Rep., 2022. [Online]. Available: https://www.iea.org/reports/world-energy-outlook-2022

[2] I. R. E. Agency, "Innovation landscape brief: Renewable Power-to-Hydrogen," *IRENA*, vol. Abu Dhabi, 2019.

[3] A. Buttler and H. Spliethoff, "Current status of water electrolysis for energy storage, grid balancing and sector coupling via power-to-gas and power-to-liquids: A review," *Renewable and Sustainable Energy Reviews*, vol. 82, no. September 2017, pp. 2440–2454, 2018. [Online]. Available: https://dx.doi.org/10.1016/j.rser.2017.09.003

[4] A. Hauch, R. Küngas, P. Blennow, A. B. Hansen, J. B. Hansen, B. V. Mathiesen, and M. B. Mogensen, "Recent advances in solid oxide cell technology for electrolysis," *Science*, vol. 370, no. 6513, p. eaba6118, oct 2020. [Online]. Available: https://dx.doi.org/10.1126/science.aba6118

[5] C. Graves, S. D. Ebbesen, S. H. Jensen, S. B. Simonsen, and M. B. Mogensen, "Eliminating degradation in solid oxide electrochemical cells by reversible operation," *Nature Materials*, vol. 14, no. 2, pp. 239–244, 2015.

[6] T. L. Skafte, O. B. Rizvandi, A. L. Smitshuysen, H. L. Frandsen, J. V. Thorvald Høgh, A. Hauch, S. K. Kær, S. S. Araya, C. Graves, M. B. Mogensen, and S. H. Jensen, "Electrothermally balanced operation of solid oxide electrolysis cells," *Journal of Power Sources*, vol. 523, 2022. [Online]. Available: http://dx.doi.org/10.10810.1016/j.jpowsour.2022.231040

[7] K. Wang, D. Hissel, M. C. Péra, N. Steiner, D. Marra, M. Sorrentino, C. Pianese, M. Monteverde, P. Cardone, and J. Saarinen, "A Review on solid oxide fuel cell models," *International Journal of Hydrogen Energy*, vol. 36, no. 12, pp. 7212–7228, 2011. [Online]. Available: http://dx.doi.org/10.1016/j.ijhydene.2011.03.051

[8] S. A. Hajimolana, M. A. Hussain, W. M. W. Daud, M. Soroush, and A. Shamiri, "Mathematical modeling of solid oxide fuel cells: A review," *Renewable and Sustainable Energy Reviews*, vol. 15, no. 4, pp. 1893–1917, 2011. [Online]. Available: http://dx.doi.org/10.1016/j.rser.2010.12.011

[9] M. García-Camprubí, S. Izquierdo, and N. Fueyo, "Challenges in the electrochemical modelling of solid oxide fuel and electrolyser cells," *Renewable and Sustainable Energy Reviews*, vol. 33, pp. 701–718, may 2014. [Online]. Available: https://dx.doi.org/10.1016/j.rser.2014.02.034

[10] D. J. R. M. Evgenij Barsoukov, *Impedance Spectroscopy: Theory, Experiment, and Applications*, 2nd ed., D. J. R. M. Evgenij Barsoukov, Ed. Hoboken, NJ, USA: John Wiley & Sons, Inc., apr 2015.

[11] Q.-A. Huang, R. Hui, B. Wang, and J. Zhang, "A review of AC impedance modeling and validation in SOFC diagnosis," *Electrochimica Acta*, vol. 52, no. 28, pp. 8144–8164, nov 2007. [Online]. Available: https://linkinghub.elsevier.com/retrieve/pii/S0013468607007505

[12] M. Schönleber and E. Ivers-Tiffée, "Approximability of impedance spectra by RC elements and implications for impedance analysis," *Electrochemistry Communications*, vol. 58, pp. 15–19, 2015. [Online]. Available: http://dx.doi.org/10.1016/j.elecom.2015.05.018

[13] B. A. Boukamp, "A Linear Kronig-Kramers Transform Test for Immittance Data Validation," *Journal of The Electrochemical Society*, vol. 142, no. 6, pp. 1885–1894, 1995. [Online]. Available: https://dx.doi.org/10.1149/1.2044210

[14] M. Schönleber, D. Klotz, and E. Ivers-Tiffée, "A Method for Improving the Robustness of linear Kramers-Kronig Validity Tests," *Electrochimica Acta*, vol. 131, pp. 20–27, 2014. [Online]. Available: http://dx.doi.org/10.1016/j.electacta.2014.01.034

[15] L. Ljung, *System Identification: Theory for the User*, ser. Prentice Hall information and system sciences series. Prentice Hall PTR, 1999. [Online]. Available: https://books.google.dk/books?id=nHFoQgAACAAJ

[16] P. Caliandro, A. Nakajo, S. Diethelm, and J. Van herle, "Model-assisted identification of solid oxide cell elementary processes by electrochemical impedance spectroscopy measurements," *Journal of Power Sources*, vol. 436, p. 226838, 2019. [Online]. Available: https://doi.org/10.1016/j.jpowsour.2019.226838

[17] G. Rinaldi, S. Diethelm, and J. Van herle, "Steam and Co-Electrolysis Sensitivity Analysis on Ni-YSZ Supported Cells," *ECS Meeting Abstracts*, vol. MA2015-03, no. 1, pp. 96–96, 2015. [Online]. Available: https://doi.org/10.1149/ma2015-03/1/96

[18] M. Mogensen, "Solid Oxide Fuel Cell Testing: Results and Interpretation," *ECS Proceedings Volumes*, vol. 1999-19, no. 1, pp. 904–915, 1999. [Online]. Available: https://dx.doi.org/10.1149/199919.0904pv